steel research international

Study on Oxide Inclusion Dissolution in Secondary Steelmaking Slags using High Temperature Confocal Scanning Laser Microscopy

Susanne Michelic,* Jürgen Goriupp, Stefan Feichtinger, Youn-Bae Kang, Christian Bernhard, and Johannes Schenk

High temperature confocal scanning laser microscopy (HT-CSLM) is used to study the dissolution behavior of Al_2O_3 inclusions in various slag compositions in the system CaO-Al_2O_3-SiO_2-MgO. This method enables the in situ observation of the dissolution at steelmaking temperatures. The change of the diameter of the spherical inclusion is measured by image analysis of pictures obtained from the HT-CSLM. Subsequently, dissolution rates and normalized dissolution curves are determined, and the governing dissolution mechanism is identified by the use of a modified approach of the diffusion equation introduced by Feichtinger et al.[27] and compared with the dissolution of SiO_2 previously reported by the same authors.[27] Finally, effective binary diffusion coefficients are calculated. Slag viscosity is shown to essentially affect the dissolution behavior, changing the normalized dissolution pattern from rather S-shaped (high slag viscosity) to a parabolic form (low slag viscosity).

1. Introduction

Nowadays, a high steel cleanness is essential not only for specific high quality applications, but is a must for a broad field of steel products. Especially for steels with increased demands regarding toughness, yield and tensile strength as well as corrosion resistance and surface quality, the content, and size of non-metallic inclusions in the steel matrix should be as low as possible. The latter can be primarily influenced in secondary metallurgical processes through purging, vacuum treatment, or the reaction and interaction with a slag phase.[1] Since the formation of non-metallic inclusions cannot be avoided completely, an efficient removal of inclusions during secondary metallurgy needs to be ensured. As far as the reaction of inclusions with slag is concerned, their separation into the slag and the subsequent inclusion dissolution in the slag are fundamental. The dissolution behavior of non-metallic inclusions can be optimized through specific design of the slag composition in dependence of the inclusion composition.

In the past, different approaches have been used to study the dissolution behavior of oxides in various slags. Before the 1990s, postmortem studies[2–4] (dipping or rotating a shaped oxide material into a liquid slag) prevailed. In the last two decades, a new method emerged enabling the in situ observation of the inclusion dissolution behavior. High temperature confocal scanning laser microscopy (HT-CSLM) offers a new approach for investigations at temperatures relevant to steelmaking processes. Based on the pioneer work done by Japanese researchers,[5] this method is applied for the investigation of phase transformations[6–9] as well as inclusion related questions like particle agglomeration in the liquid steel[10,11] or reactions of inclusions with slag and refractory material.[12–14] Meanwhile, also several publications dealing with the use of HT-CSLM for dissolution studies exist.[15–27] The main focus of previous analyses lies on the dissolution of Al_2O_3, MgO, and $MgAl_2O_4$ in CaO-Al_2O_3-SiO_2 or CaO-Al_2O_3-SiO_2-MgO slags. For the determination of the governing dissolution mechanism, different models are proposed in literature: the analytical solution using the Shrinking Core Model (SCM) has been widely applied.[15,16,18,19,21] In this model, either the chemical reaction at the interface between inclusion and slag or the mass transport of the dissolving particle in the boundary layer of the slag can be the rate controlling

[*] Prof. S. Michelic, J. Goriupp, S. Feichtinger, Prof. C. Bernhard, Prof. J. Schenk
Chair of Ferrous Metallurgy, Montanuniversitaet Leoben, Leoben 8700, Austria
Email: susanne.michelic@unileoben.ac.at
Prof. Y.-B. Kang
Graduate Institute of Ferrous Technology, Pohang University of Science and Technology (POSTECH), Pohang, Kyungbuk 790-784, Korea

DOI: 10.1002/srin.201500102

step for the dissolution. Some years ago, Verhaeghe et al.[22–26] proposed a new approach using a diffusion equation coupled with Lattice Boltzmann modeling. Although the latter offers more possibilities, it is less applied due to the high computational effort needed. A modified diffusion model based on the use of well-shaped spherical particles was introduced by Feichtinger et al.[27] It focuses on the influence of slag viscosity on the governing dissolution mechanism. As equally assumed for all other mentioned models, the formation of a solid layer around the inclusion during dissolution cannot be considered with this approach.

In the present work, the application of CSLM for dissolution studies including the determination of dissolution mechanisms according to the approach proposed by Feichtinger et al.[27] is shown for two different slag/inclusion systems: on the one hand, the dissolution of SiO_2 particles in $CaO\text{-}Al_2O_3\text{-}SiO_2$ slags important for the production of steel wire and tire cord is demonstrated;[27] on the other hand a more general system, i.e., the dissolution of Al_2O_3 in $CaO\text{-}Al_2O_3\text{-}MgO\text{-}SiO_2$ ladle slags, is discussed. Next to an absolute comparison of dissolution rates for different slag compositions and the explanation of governing dissolution mechanisms, the significance of slag viscosity and the calculation of diffusion coefficients are shown.

2. High Temperature Confocal Scanning Laser Microscopy (HT-CSLM)

2.1. Experimental Set-Up and Procedure

At the Chair of Ferrous Metallurgy at the Montanuniversitaet Leoben, a Confocal Scanning Laser Microscope type VL2000DX from Lasertec and a high temperature furnace type SVF17-SP from Yonekura are available. The decisive advantage of HT-CSLM in contrast to conventional microscopes or experimental facilities is the possibility of in situ observations at temperatures up to 1700 °C in combination with very good image quality. This is primarily possible due to the following aspects:[28]

1. A laser is used as a light source characterized by a wavelength of 408 nm and therewith below the thermal radiation spectrum of the observed samples. So, the contrast of the image can be increased significantly.
2. Heat is provided by a halogen lamp with a maximum power of 1500 W. In combination with a low sample weight, this enables heating rates up to 1200 °C and cooling rates of 1000 °C min^{-1}.
3. The maximum operating temperature is only limited by the thermocouple type and is about 1700 °C for standard configurations. Since the high temperature furnace is cooled, the thermal strain for the furnace through the radiation source is comparably low.
4. Through the use of an acousto-optic element, a very high scan rate can be reached. For the maximum resolution of 1024×1024, 15 images per second are stored. A resolution of 1024×256 enables the recording of 60 images per second.

Figure 1 illustrates the schematic view of the experimental set-up in the high temperature furnace which shows an elliptic, gold-coated inner contour. The halogen lamp is situated in the bottom focal point. The sample holder with the crucible containing the sample is located in the top focal point of the ellipse. The temperature is measured with a thermocouple fixed at the bottom side of the sample holder. The position of the thermocouple inevitably results in a temperature difference between the sample surface and the thermocouple. Therefore, an accurate temperature calibration is necessary before the experiment.

Figure 2 gives an overview on the experimental procedure regarding experiments studying the dissolution behavior of non-metallic inclusions in slags. In principle, every experiment consists of three main steps: slag preparation, dissolution experiment in the CSLM, and the subsequent data evaluation. Details concerning slag pre-treatment as well as the adjustment of the temperature measurement can be found elsewhere.[27]

Figure 3a shows the sample holder and the experimental configuration in detail: for all experiments in which a slag phase is involved, platinum crucibles are used. For dissolution experiments, a well-shaped spherical inclusion particle with a known diameter is placed on the surface of the defined amount of pre-molten slag in the crucible. Figure 3b shows a typical heating cycle for dissolution experiments. The whole assembly is heated up to the target temperature using the maximum heating rate. This is important to ensure that the inclusion hardly starts to dissolve before the experimental temperature is reached. At a temperature 50 °C below the final temperature, the heating rate is reduced to 100 °C min^{-1} in order to avoid overshooting. Most dissolution experiments are performed at an experimental temperature of 1600 °C

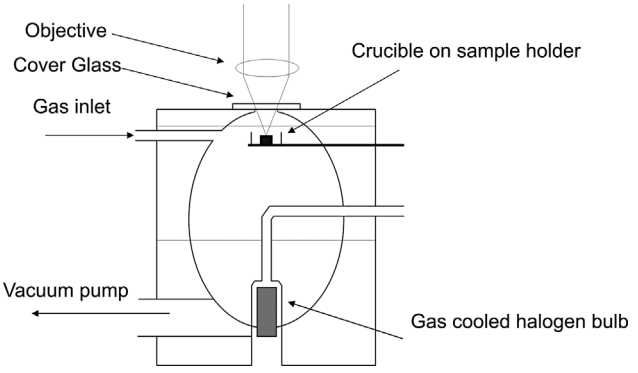

Figure 1. Schematic view of the high temperature furnace.

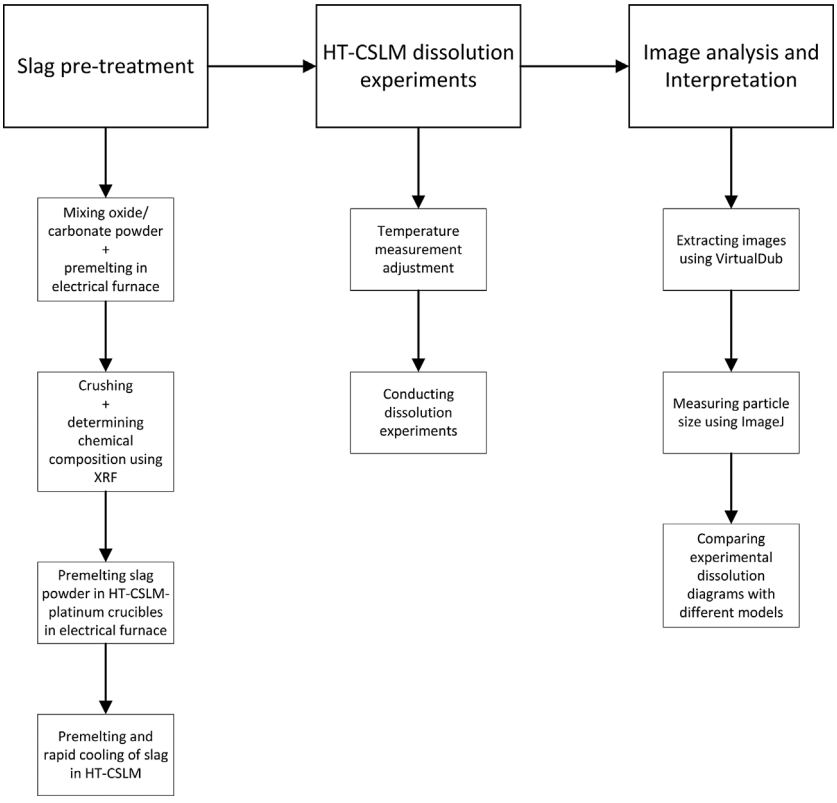

Figure 2. Flow chart of experimental procedure.

since this is usually the most interesting temperature for steelmaking processes. Nevertheless, experimental temperatures can be defined arbitrarily up to 1700 °C. As demonstrated in Figure 3b, in the present study, experiments for the Al_2O_3 dissolution (system 2) are conducted at 1600 °C. High purity argon with a flow rate of 100 cm^3 min^{-1} ensures a neutral atmosphere in the furnace. Since the particle weight is less than 0.01% of the slag weight, composition changes by the dissolution of the particle are regarded as negligible.

2.2. Data Evaluation

The output of the dissolution experiment in CSLM is a conventional video clip. As a first step, the video is

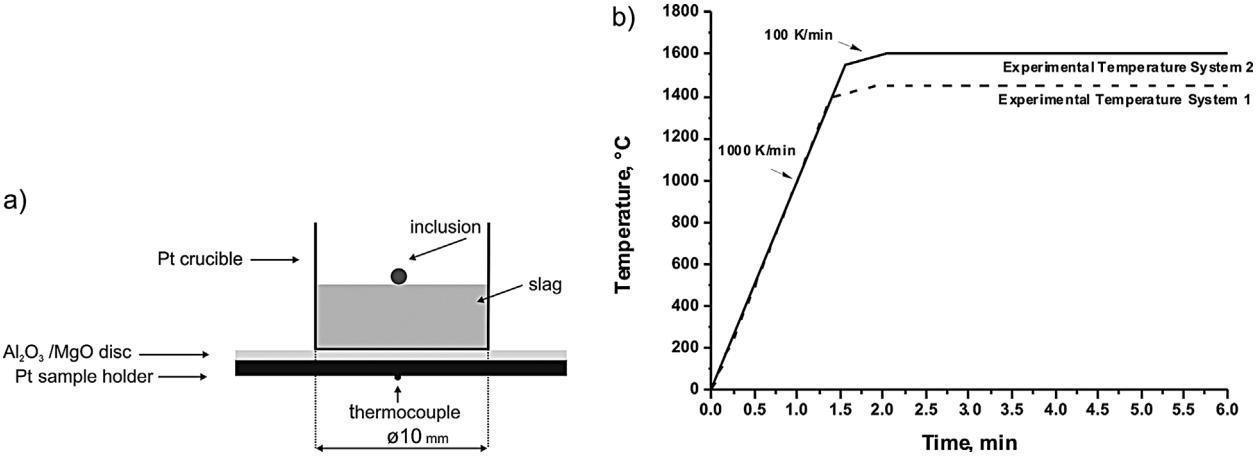

Figure 3. a) Schematic view of the experimental set-up for dissolution experiments. b) Time-temperature profile of dissolution experiments.

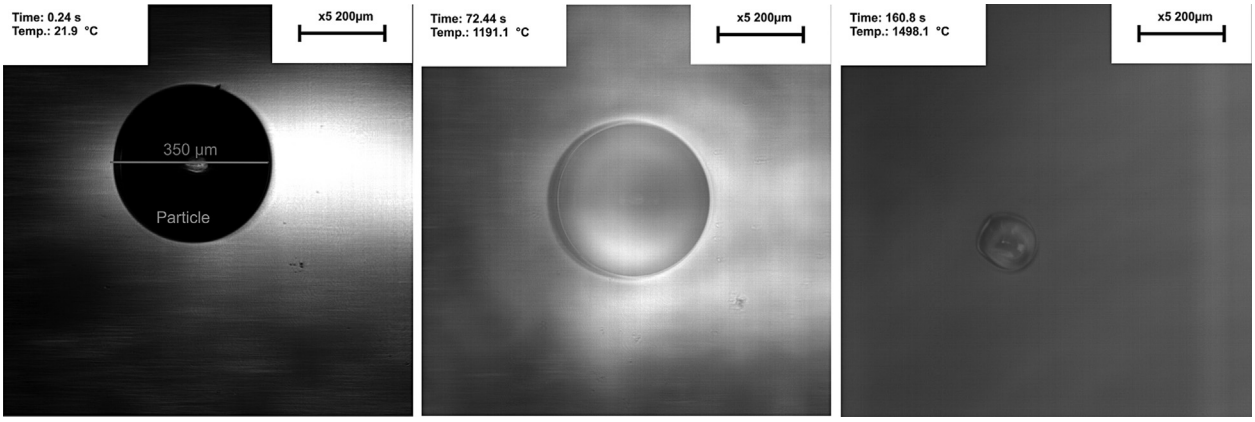

Figure 4. Video screenshots of dissolving inclusion during an experiment.

converted into pictures by using the public domain software VirtualDub.[29] Secondly, the pictures are analyzed by the public domain image analysis software ImageJ.[30] **Figure 4** gives examples of pictures from the CSLM showing an SiO_2 particle dissolving in the slag phase (CaO-Al_2O_3-SiO_2) with ongoing time, which were not shown in the authors' previous publication.[27] For the analysis of the dissolution behavior, a boarder is manually drawn around the dissolving inclusion and the area of the particle is determined. Finally, an equivalent particle diameter is calculated assuming that the particle shape remains spherical throughout the experiment. The time when the experimental temperature has been reached is defined as time zero for all further evaluations. All slags were fully molten at time zero, achieving their liquidus temperatures around 1400 °C at the latest (depending on the slag composition). For Al_2O_3 experiments, all particles were fully submerged at the experimental temperature. For SiO_2, the particles have been mostly wetted and were floating in the slag at experimental temperature. In order to focus on possible dissolution before the defined experimental temperature, in every experiment, the particle diameter was measured as soon as the experimental temperature has been reached. A comparison with the initial particle diameter does not show large deviations in any investigated case. However, a certain reaction before the experimental temperature can neither be excluded nor prohibited due to the finite heating rates.

3. Determination of Dissolution Mechanisms

Based on the evaluated data, absolute dissolution rates (diameter versus time) or normalized dissolution graphs (transient diameter divided by initial diameter and time divided by total dissolution time) are analyzed. The latter also serve for the determination of the related dissolution mechanism. As far as dissolution mechanisms are concerned, different approaches are widely published.[15–27] The SCM is an analytical solution for the determination of the rate controlling dissolution mechanism typically resulting in a linear correlation between particle size and dissolution time (reaction rate control) or a parabolic dependence (mass transfer control). Using this model, it is presumed that the slag is saturated with the dissolving species at the interface between the slag and the dissolving particle. The saturation or equilibrium concentration of the dissolving species is obtained by available phase diagrams or by thermodynamic calculations under the assumption of a straight dissolution path. Further details of this model are given in the literature.[31]

Although an analytical solution using the SCM is sufficient in many cases, some experimental results cannot be described satisfactorily. Thus, numerical solutions of the diffusion equation (diffusion into a stagnant fluid) have to be applied.[22–26] Approximations of the diffusion equation for spherical particles are suited to analyze if the dissolution is governed by diffusion or not. Dissolution controlled by diffusion in a stagnant fluid can generally be described by Fick's first and second law of diffusion.[32–34] Principally, two different approximations have to be distinguished:

Stationary interface or invariant interface approximations: It is assumed that the diffusion field is not altered by the movement of the interface between particle and a viscous slag (S-shaped normalized dissolution curve):

$$\frac{dR}{dt} = -\frac{k \cdot D}{R} - k \cdot \sqrt{\frac{D}{\pi \cdot t}} \tag{1}$$

where R is the radius of the particle, D is an effective binary diffusion coefficient of a particle in the slag, and t is time. The dimensionless saturation k is defined as follows:

$$k = \frac{c_{sat} - c_0}{c_{incl} - c_{sat}} \tag{2}$$

The inclusion concentrations in the dimension kg m^{-3} are obtained as follows, where x is a mass fraction of the inclusion in the slag and ρ is the slag density in kg m^{-3}:

$$c = x \cdot \rho \tag{3}$$

Invariant field approximation: The time-dependent change of the concentration profile in a less viscous slag is neglected (parabolic normalized dissolution curve):

$$\frac{dR}{dt} = -\frac{k \cdot D}{R} \tag{4}$$

Details regarding the two cases as well as the complete derivation can be found in a previous publication.[27] For the evaluation of the governing dissolution mechanism, at the Chair of Ferrous Metallurgy, a modified model presented by Feichtinger et al.[27] is applied merging the two approaches described above and introducing an additional factor f to the second term of Equation 1:

$$\frac{dR}{dt} = -\frac{k \cdot D}{R} - f \cdot k \cdot \sqrt{\frac{D}{\pi \cdot t}} \tag{5}$$

This modified model especially considers the influence of slag viscosity on the normalized dissolution pattern. For $f = 1$, which is the case for slags with infinitely high viscosity, the modified model turns into the invariant interface approximation (Equation 1) resulting in an S-shaped dissolution curve. In contrast, for slags with infinitely low viscosity, f equals 0 and the modified model reduces to the invariant field approximation (Equation 4) resulting in a parabolic dissolution curve.

4. Examples of Application

4.1. Investigated Inclusions and Slags

The experimental procedure and the subsequent data evaluation described in Section 2 are now examined using two examples of secondary metallurgy. Two different slag systems are studied. On the one hand, the dissolution of SiO_2 inclusions is analyzed in the system CaO-Al_2O_3-SiO_2. Detailed results of this investigation have been published previously.[27] In the present paper, only selected examples are given for reasons of comparison. On the other hand, Al_2O_3 dissolution is studied in CaO-Al_2O_3-SiO_2 slags with significant MgO contents. All investigated slag compositions are summarized in **Table 1**. All experiments have been performed with well-shaped spherical particles (made by Sandoz Fils, Cugy, Switzerland) following the procedure shown in Figure 2 and the time temperature profile given in Figure 3b. For experiments in system 1, SiO_2 particles with a diameter of 350 μm and a density of 2.20 g cm^{-3} are used; for system 2 experiments, the initial Al_2O_3 diameter is 400 μm (density of 3.98 g cm^{-3}). These values are given by the supplier. The stated purity of both particle types is quoted with 99.99%. Neither the content of impurities nor the density has been evaluated experimentally by the authors. The difference in experimental temperature is explained by the significantly faster dissolution of SiO_2 compared to Al_2O_3. A collection of slag densities can be found in Slag Atlas.[35] The bulk slag concentrations c_0 were analyzed by XRF, whereas the saturation concentrations c_{sat} for SiO_2 and Al_2O_3 as well as the activities in the slags are calculated by FactSage.[36] For the determination of slag viscosities, it is referred to literature.[27,37] More details regarding thermodynamic

	ID	CaO [wt%]	Al_2O_3 [wt%]	SiO_2 [wt%]	MgO [wt%]	Particle type	Temperature [°C]
System 1[27]	Slag 1.1	34.1	10.6	54.6	0	SiO_2	1450
	Slag 1.2	38.3	10.6	50.5	0	SiO_2	1450
	Slag 1.5	36.4	26.5	37.1	0	SiO_2	1450
	Slag 1.6	38.8	18.9	42.3	0	SiO_2	1450
	Slag 1.3	43.7	10.4	45.3	0	SiO_2	1450
	Slag 1.4	46.6	10.8	42.8	0	SiO_2	1450
System 2	Slag 2.1	28.1	37.4	28.1	6.4	Al_2O_3	1600
	Slag 2.2	37.0	37.0	18.5	7.5	Al_2O_3	1600
	Slag 2.3	46.0	27.6	18.4	8.0	Al_2O_3	1600
	Slag 2.4	57.2	19.1	19.1	4.6	Al_2O_3	1600
	Slag 2.5	33.6	16.8	33.6	16.0	Al_2O_3	1600

Table 1. Overview on investigated slag compositions within the system CaO-Al_2O_3-MgO-SiO_2.

	ID	a SiO_2	$(wt\%SiO_2)_{sat}$	k	Viscosity [Pa · s]
			All values for $T = 1450\,^{\circ}C$		
System 1[27]	Slag 1.1	0.46	67.60	0.94	2.41
	Slag 1.2	0.31	67.30	1.19	1.25
	Slag 1.5	0.09	70.50	3.03	1.08
	Slag 1.6	0.14	69.10	2.17	1.02
	Slag 1.3	0.16	66.90	1.48	0.60
	Slag 1.4	0.10	66.80	1.64	0.47
	ID	**a Al_2O_3**	**$(wt\%Al_2O_3)_{sat}$**	**k**	**Viscosity [Pa · s]**
			All values for $T = 1600\,^{\circ}C$		
System 2	Slag 2.1	0.43	42.00	0.04	0.55
	Slag 2.2	0.15	38.40	0.01	0.25
	Slag 2.3	0.05	49.86	0.22	0.18
	Slag 2.4	0.01	58.55	0.42	0.18
	Slag 2.5	0.06	22.46	0.04	0.18

Table 2. Calculated thermodynamic data for investigated slags.

considerations in the investigated slag systems are published elsewhere.[27,38] All calculated results are demonstrated in **Table 2**.

As already mentioned, all described models are based on the assumption that no solid layer is formed around the dissolving particle. For none of the investigated slags in this study the formation of a solid layer during dissolution has been observed. A representative micrograph of a dissolving SiO_2 particle in a CaO-Al_2O_3-SiO_2 slag including a line scan through the particle area can be found in a previous publication.[27] For each slag, the same experiments are repeated three times in order to confirm reproducibility. An example of repeatability of the experiments (SiO_2 dissolution in system 1) can also be found in ref.[27]

An aspect which has to be considered is the movement of the particle during the experiment which can affect the dissolution behavior. Regarding the Al_2O_3 dissolution experiments, the particle principally remained in the bulk slag. However, especially for the low viscosity slags in system 2, the particle tends to drop to the bottom of the crucible with ongoing dissolution time. Since the dissolution rate for the low viscosity slags in system 2 is comparably fast, this aspect is seen to be negligible in the present study. Regarding the SiO_2 dissolution experiments, the particles float on the slag surface throughout the dissolution due to the lower density of the inclusions compared to the density of the slag. It cannot be avoided that a small area of the inclusion is not wetted with the slag. This fact also can influence the dissolution rate. At present, the experimental set-up and procedure does not allow to prohibit particle movement during the experiment, since this can be different for every slag/particle combination. However, this will be in the author's focus of interest for further investigations.

4.2. SiO_2 Dissolution in CaO-Al_2O_3-SiO_2 Slags

Figure 5 illustrates selected results for absolute dissolution rates as well as normalized dissolution curves for system 1. Figure 5a demonstrates the average dissolution rates for SiO_2 inclusions in slags 1.1, 1.3, and 1.6 which are characterized by different slag viscosities. All absolute dissolution times are below 250 s. This is a comparably fast dissolution rate especially considering the low experimental temperature. Thus, a relatively fast SiO_2 dissolution at industrial steelmaking temperatures can be assumed.

Comparing the dissolution rates for slags 1.1, 1.3, and 1.6 concludes in a decreasing dissolution rate with increasing slag viscosity. Normalized dissolution curves for SiO_2 in slags 1.1 (highest viscosity) and 1.4 (lowest viscosity) are demonstrated in Figure 5b. Additionally, the curves for the invariant field approximation (parabolic shape), the invariant interface approximation (S-shaped curve), as well as the linear relationship for the reaction rate-controlled dependence are plotted. It can be seen that the dissolution path of SiO_2 in slag 1.1 is rather S-shaped than parabolic. In contrast, the dissolution pattern of SiO_2

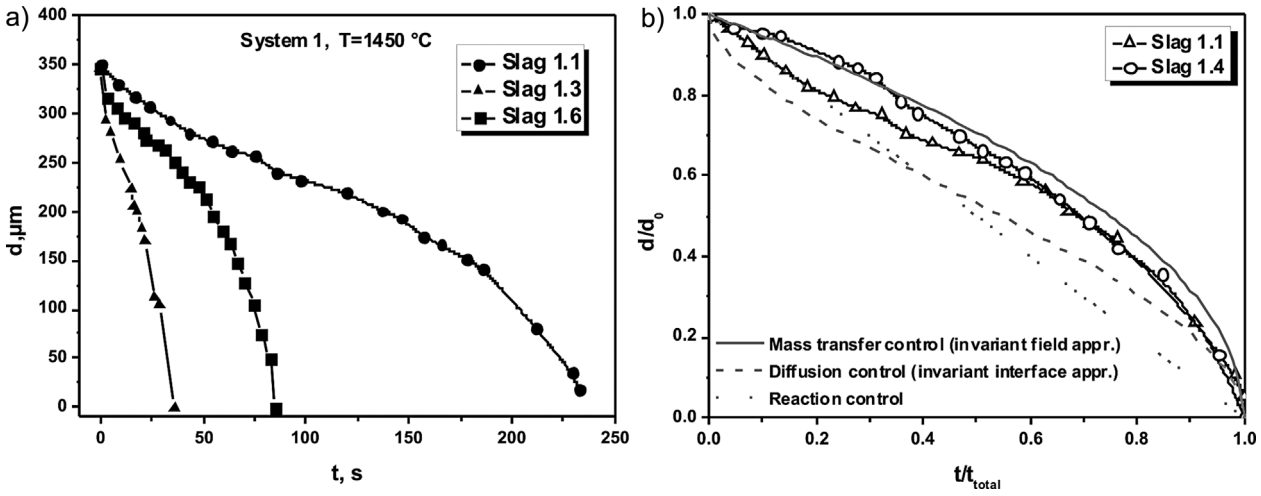

Figure 5. a) Dissolution rates of SiO_2 in selected slags of system 1. b) Normalized dissolution curves for slags 1.1 and 1.4 compared to commonly applied dissolution models.[27]

in slag 1.4 shows a more parabolic shape. However, none of the investigated slags is in perfect agreement with one of the proposed models.

So far, no other in situ observations studying the dissolution behavior of SiO_2 have been published to the best of authors' knowledge. However, ex situ studies of the dissolution of fused SiO_2 exist.[2] In the latter case, boundary layer diffusion was determined to be the governing dissolution mechanism. In order to describe the dissolution behavior more clearly, the modified approach of Feichtinger et al.[27] is applied. Detailed results for slags 1.1–1.6 using the modified approach with the *f*-factor are shown in a previous publication.[27] Summing up, the following relationship has been determined: slags with high viscosity resulting in a rather S-shaped curve are also characterized by a high *f*-factor. In contrast, for slags with lower viscosity and parabolic shape, the *f*-factor is decreased.

4.3. Al_2O_3 Dissolution in CaO-Al_2O_3-SiO_2-MgO Slags

A comparison of absolute dissolution rates for selected slags of system 2 is given in **Figure 6**. As already shown for system 1 in Figure 5a, slag viscosity essentially influences the absolute dissolution time. Al_2O_3 dissolves significantly faster in slag 2.2 and 2.4 than in slag 2.1 (see Figure 6a). It is necessary to mention that the dissolution path for slag 2.1 has been extrapolated from 750 s to the end since the measurement was interrupted due to an overload in collected data.

Although several researchers have already studied the dissolution of Al_2O_3 in situ by means of HT-CLSM,[16,17,19] an exact comparison with literature is difficult due to differences in slag composition as well as experimental temperatures. Furthermore, it has to be clarified that a direct comparison between dissolution rates in systems 1 and 2 is not the aim of this study. It also does not seem

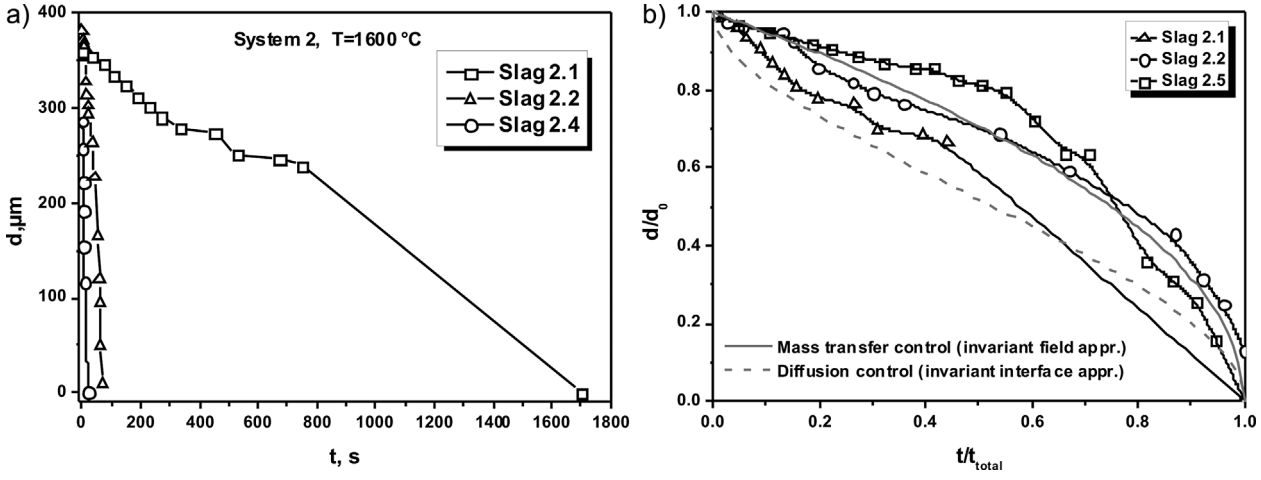

Figure 6. a) Dissolution rates of Al_2O_3 in selected slags of system 2. b) Normalized dissolution curves for slags 2.1, 2.2, and 2.5 in comparison with commonly applied dissolution models.

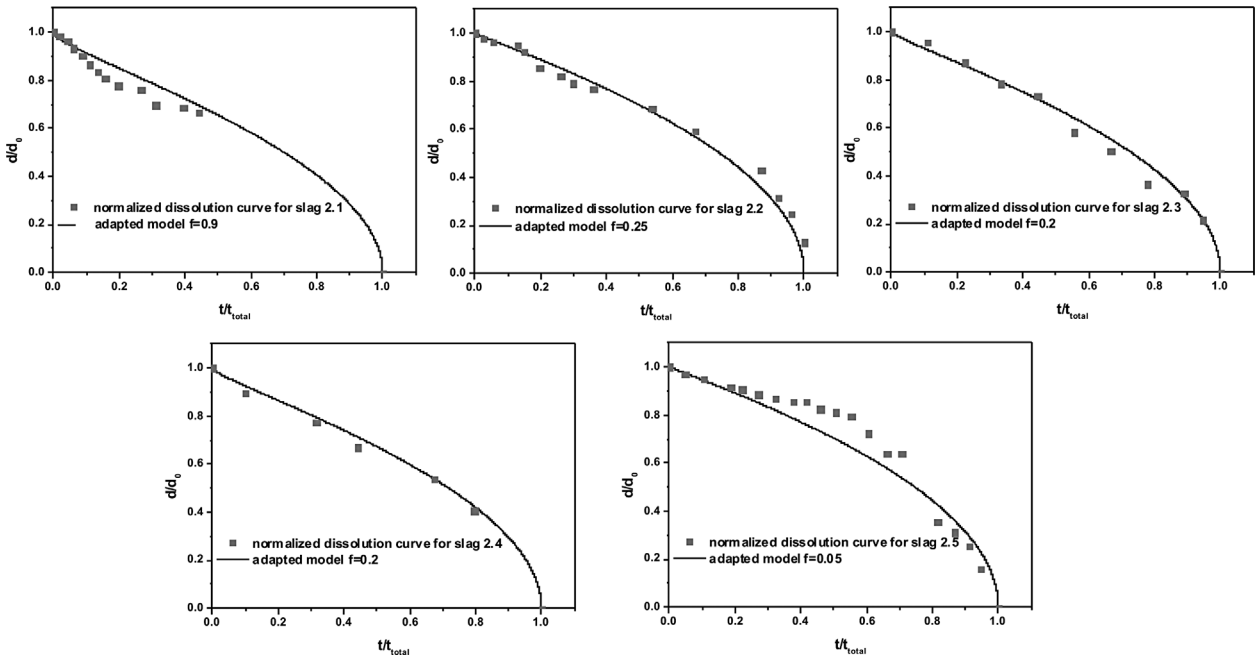

Figure 7. Adapted model calculations for all slags of system 2.

reasonable due to different initial conditions (particle size and temperature) as well as the significant differences in slag compositions.

Figure 6b demonstrates the normalized dissolution curves for slags 2.1, 2.2, and 2.5 in comparison with commonly applied dissolution models. The results show the same trend as observed for SiO_2 dissolution in system 1 regarding the influence of slag viscosity: a transition from S-shape for slags with high viscosity (2.1) toward a parabolic-like curve for slags with lower viscosity (2.5) is observed. The reaction rate-controlled linear dependence is not plotted in the present case since this relationship seems to be far away from reality for all slags in this study.

Figure 7 summarizes the results for all investigated dissolution patterns in system 2 by means of the model of Feichtinger et al.[18] including the applied *f*-factors for each slag. The same dependence between slag viscosity and *f* as found for SiO_2 dissolution in system 1 (see previous work in ref.[27]) can be observed; similar to slag 1.4, slag 2.5 is characterized by the lowest *f*-factor in system 2 which reflects a parabolic shape of the pattern. Slag 2.1 shows an *f*-factor close to 1 which reflects a nearly S-shaped curve. Slags 2.3, 2.4, and 2.5 have the same viscosity, but different chemical composition. For slags 2.3 and 2.4, the same *f*-factor is found, which underlies the close relation between slag viscosity and dissolution mechanism. However, regarding slag 2.5, an *f*-factor of almost 0 is observed. The latter slag is characterized by an MgO content of 16 wt%, which is the highest among the investigated slags and is supposed to essentially affect the dissolution behavior. Further studies are necessary to critically analyze this influencing parameter.

4.4. Influence of Slag Viscosity

Investigations of SiO_2 and Al_2O_3 dissolution in different slag systems proved the significant influence of slag viscosity on the dissolution behavior. In **Figure 8**, the *f*-factor is plotted versus slag viscosity for each slag of the two systems. A linear dependence between *f* and slag viscosity has already been reported previously by the authors for SiO_2 dissolution in $CaO\text{-}Al_2O_3\text{-}SiO_2$ slags at 1450 °C.[27] Also, for the dissolution of Al_2O_3 in $CaO\text{-}Al_2O_3\text{-}MgO\text{-}SiO_2$ slags at 1600 °C, a linear dependence, characterized by a sharper slope compared to slags in system 1, is

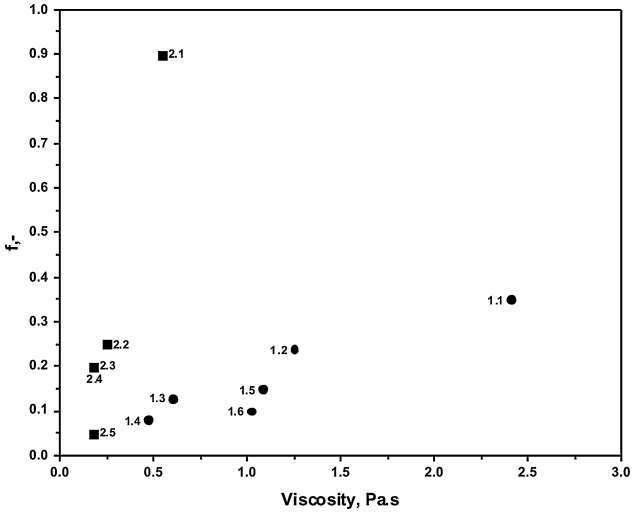

Figure 8. Relationship between the *f*-factor and the slag viscosity for all investigated slags in systems 1 and 2.

observed. Despite the lower range of the viscosities of system 2, the fit parameters *f* show similar (slags 2.2–2.5) or even higher values (slag 2.1). This might be attributed to the higher density of the Al_2O_3 particles, resulting in less movement of the particle during the experiment, i.e., a more stable development of the diffusion field around the particle. However, the reason is not clarified in detail at the present stage. Further experiments at varying temperatures and slag viscosities have to be carried out in order to get more data to characterize this relationship.

4.5. Diffusion Coefficients

Based on the modified model approach, also the effective binary diffusion coefficients can be calculated. That means that the system is reduced to a pseudo binary system consisting of the considered diffusion component and the slag consisting of the remaining components. All calculation results are summarized in **Table 3**. The diffusion coefficients for SiO_2 are in the same range as previously published values which are based on ex situ studies.[2] Samaddar et al.[2] reported a value of 4.5×10^{-12} m^2 s^{-1} for the diffusion coefficient of SiO_2 in a 40%CaO-20%Al_2O_3-40%SiO_2 slag at 1425 °C. Also, Majdic and Wagner[39] investigated the diffusion coefficient of SiO_2 in various slags at different temperatures. For a 38.5%CaO-16.5%Al_2O_3-45%SiO_2 slag – which represents a similar composition as slag 1.6 – an SiO_2 diffusion coefficient of 2.8×10^{-10} m^2 s^{-1} at 1500 °C was determined. The value found for slag 1.6 in the present calculations (see Table 3) lies in the range of the two mentioned publications. Recently, investigations regarding the dissolution rate and diffusivity of Silica in SiMn slags in the temperature range between 1400 and 1550 °C have been published by Maroufi et al.[40] They used a rotating disk/cylinder technique in order to examine the effect of temperature and slag composition on the dissolution behavior. Comparing their results to the values calculated in this study also shows a good agreement. For example, an SiO_2 diffusion coefficient of 8.4×10^{-11} m^2 s^{-1} was found for a 40.8%SiO_2-11.3%Al_2O_3-13.9%MnO-26.5%CaO-5%MgO-2.4%K_2O slag at 1400 °C. This composition resembles slag 1.6 concerning the three main components SiO_2, Al_2O_3, and CaO. The determined diffusion coefficient lies in a comparable range.

Table 3 also summarizes the effective binary diffusion coefficients for Al_2O_3 at 1600 °C for the investigated slags in system 2. There are several published values for Al_2O_3 diffusion coefficients in various slags available in the literature[16,17] which are also based on experiments using the CSLM. But, a direct comparison with published values still proved to be difficult, since the MgO content of slags in system 2 is comparably high and MgO significantly influences slag viscosity. For example, Monaghan and Chen[16] also investigated the dissolution behavior of Al_2O_3 in CaO-Al_2O_3-SiO_2 slags at 1600 °C. The related slag viscosities lied in the range between 1 and 10 Pa·s, whereas slag viscosities in the present study are below 1 Pa·s for system 2. Nevertheless, it was tried to validate the diffusion coefficients calculated in the present study. For this purpose, an equation proposed by Monaghan et al.[16] was used. This equation is based on a linear regression fit of CSLM experimental dissolution data also considering the concentration of the dissolving species in the bulk, its saturation concentration, particle density, and particle radius. Applying this equation for the calculation of the Al_2O_3 diffusion coefficient in slags in the present study yields similar results as given in Table 3 according to the approach of Feichtinger et al.[27] As an example, the calculated Al_2O_3 diffusion coefficient in slag 2.4 is determined with 1.94×10^{-09} m^2 s^{-1} in the present study. Using the equation given by Monaghan and Chen[16] would result in a value of 2.44×10^{-09} m^2 s^{-1}. So, both approaches are seen to be well suited for the calculation of diffusion coefficients.

Diffusion coefficient *D*			
***D* for SiO_2, $T = 1450$ °C**		***D* for Al_2O_3, $T = 1600$ °C**	
System 1	**m^2 s^{-1}**	**System 2**	**m^2 s^{-1}**
Slag 1.1	4.44×10^{-11}	Slag 2.1	1.45×10^{-10}
Slag 1.2	8.49×10^{-11}	Slag 2.2	4.11×10^{-12}
Slag 1.5	3.79×10^{-11}	Slag 2.3	1.45×10^{-09}
Slag 1.6	6.03×10^{-11}	Slag 2.4	1.94×10^{-09}
Slag 1.3	1.80×10^{-10}	Slag 2.5	3.38×10^{-09}
Slag 1.4	2.38×10^{-10}		

Table 3. Calculated effective binary diffusion coefficients for all investigated slags.

5. Conclusions

HT-CSLM is presented as a well-suited method for the in situ observation of inclusion dissolution in various slag compositions. The very well-controllable experimental conditions enable a detailed study of the dissolution behavior. Absolute dissolution rates as well as dissolution mechanisms can be examined and quantified using a modified approach of the diffusion equation introduced by Feichtinger et al.[27] Diffusion coefficients can be calculated based on this modified approach. Two different applications are described. The following conclusions are drawn:

1. The dissolution of SiO_2 in CaO-Al_2O_3-SiO_2 slags is observed to be very fast compared to other inclusion types described in the literature. For SiO_2, no

comparable in situ data are available in literature. Ex situ studies confirm the fast dissolution of SiO_2. Commonly applied models are not in perfect agreement with the observed normalized dissolution pattern. Applying the modified approach with the introduced *f*-factor yields significantly better results.[27]

2. The dissolution of Al_2O_3 in the CaO-Al_2O_3-SiO_2-MgO system shows similar results as already published in the literature regarding the dissolution rate as long as the MgO-content is not too high. Increased slag viscosities essentially extend the dissolution time. The dissolution behavior is also described by the use of the *f*-factor.
3. Slag viscosity is proved to be an essential influencing factor for both described systems. Slags with higher viscosity tend to show a slightly S-shaped normalized dissolution curve, whereas slags with lower viscosity are characterized by a parabolic pattern. Within both systems, a linear dependence between *f* and slag viscosity is observed. However, the slopes are significantly different for the both systems. The difference in particle density in relation to slag density, the different experimental temperature, as well as the MgO content in the slags might be possible explanations for this difference. However, further experiments are necessary to clarify this aspect.
4. Based on the described modified approach effective binary diffusion coefficients can be calculated. The obtained results are in good accordance with values published based on postmortem studies using rotating dip techniques (for SiO_2 dissolution in system 1) as well with values calculated based on an approach proposed by Monaghan and Chen[16] (for Al_2O_3 dissolution in system 2).

Acknowledgements

Financial support by the Austrian Federal Government and the Styrian Provincial Government, represented by Österreichische Forschungsförderungsgesellschaft mbH and by Steirische Wirtschaftsförderungsgesellschaft mbH within the research activities of the K2 Competence Centre on "Integrated Research in Materials, Processing and Product Engineering," operated by the Materials Center Leoben Forschung GmbH in the framework of the Austrian COMET Competence Centre Programme, is gratefully acknowledged. The financial support is also gratefully acknowledged by K1-Met, also a member of the COMET-Competence Centers for Excellent Technologies and supported by the BMVIT, BMVITJ, the Provinces of Upper Austria, Styria and Tyrol, SFG and Tiroler Zukunftsstiftung. COMET is managed by FFG (Austrian research promotion agency).

Received: March 23, 2015

Keywords: non-metallic inclusion; dissolution; slag; CaO-Al_2O_3-SiO_2-MgO; confocal scanning laser microscopy

References

[1] A. Gosh, *Secondary Metallurgy*, CRC Press, Boca Raton, FL **2001**.
[2] B. N. Samaddar, W. D. Kingery, A. R. Cooper, *J. Am. Ceram. Soc.* **1964**, *47*, 5.
[3] X. Yu, R. J. Pomfret, K. S. Coley, *Metall. Mater. Trans. B* **1997**, *28*, 2.
[4] S. Taira, K. Nakashima, K. Mori, *ISIJ Int.* **1993**, *33*, 1.
[5] H. Chikama, H. Shibata, T. Emi, M. Suzuki, *Mater. Trans. JIM* **1997**, *37*, 4.
[6] M. Reid, R. J. Dipenaar, *ISIJ Int.* **2004**, *44*, 565.
[7] D. Phelan, M. Reid, R. J. Dipenaar, *Mater. Sci. Eng.* **2008**, *477A*, 226.
[8] D. Phelan, M. Reid, R. J. Dipenaar, *Comp. Mater. Sci.* **2005**, *34*, 282.
[9] Z. Liu, Y. Kobayashi, J. Yang, K. Nagai, M. Kuwabara, *ISIJ Int.* **2006**, 46.
[10] H. Yin, H. Shibata, T. Emi, M. Suzuki, *ISIJ Int.* **1997**, *37*, 10.
[11] H. Shibata, H. Yin, H. S. Yoshinaga, T. Emi, M. Suzuki, *ISIJ Int.* **1998**, *38*, 2.
[12] P. Misra, *Metall. Mater. Trans. B* **2000**, *31*, 5.
[13] S. Sridhar, in *Proc. of the 3rd International Conference on the Science and Technology of Steelmaking*, Charlotte (NC), USA.
[14] S. Michelic, C. Bernhard, M. Hartl, in *Inclusion Symp. der AISTech 2011*, Indianapolis, USA.
[15] J. Liu, M. Guo, P.T. Jones, F. Verhaeghe, B. Blanpain, P. Wollants, *J. Eur. Ceram. Soc.* **2007**, *27*, 4.
[16] B. J. Monaghan, L. Chen, *J. Non-Cryst. Solids* **2004**, *347*, 1.
[17] J. Liu, F. Verhaeghe, M. Guo, B. Blanpain, P. Wollants, *J. Am. Cer. Soc.* **2007**, *90*, 12.
[18] B. J. Monaghan, L. Chen, *Ironmaking Steelmaking* **2008**, *33*, 4.
[19] S. Sridhar, A. W. Cramb, *Metall. Mater. Trans. B* **2000**, *31*, 2.
[20] K. W. Yi, C. Tse, J. H. Park, M. Valdez, A. W. Cramb, S. Sridhar, *Scand. J. Metall.* **2003**, *32*, 4.
[21] A. Fox, M. Valdez, J. Gisby, R. Atwood, P. Lee, S. Sridhar, *ISIJ Int.* **2004**, *44*, 5.
[22] F. Verhaeghe, S. Arnout, B. Blanpain, P. Wollants, *Phys. Rev. E* **2005**, *72*, 3.
[23] F. Verhaeghe, B. Blanpain, P. Wollants, *Modell. Simul. Mater. Sci. Eng.* **2008**, *16*, 4.
[24] F. Verhaeghe, J. Liu, M. Guo, S. Arnout, B. Blanpain, P. Wollants, *J. Appl. Phys.* **2008**, *103*, 2.
[25] F. Verhaeghe, J. Liu, M. Guo, S. Arnout, B. Blanpain, P. Wollants, *Appl. Phys. Lett.* **2007**, *91*, 12.
[26] F. Verhaeghe, S. Arnout, B. Blanpain, P. Wollants, *Phys. Rev. E* **2006**, *73*, 3.
[27] S. Feichtinger, S. K. Michelic, Y.-B. Kang, C. Bernhard, *J. Am. Ceram. Soc.* **2014**, *97*, 316.
[28] C. Bernhard, S. Schider, A. Sormann, G. Xia, S. Ilie, *Berg-Huettenmaenn. Monatsh.* **2011**, *156*, 5.

[29] VirtualDub, version 1.9.10, developed by A. Lee and available on the internet at IR http://www., virtualdub., org/, accessed: February **2015**.
[30] ImageJ, version 1.45s, developed at U.S. National Institutes of Health and available on the internet at http://imagej.nih.gov/ij/, accessed: February **2015**.
[31] O. Levenspiel, *Chemical Reaction Engineering*, 3rd ed., John Wiley & Sons, New York **1999**.
[32] M. J. Whelan, *Met. Sci. J.* **1996**, *3*, 1.
[33] H. B. Aaron, G. R. Kotler, *Metall. Trans.* **1971**, *2*, 2.
[34] L. C. Brown, *J. Appl. Phys.* **1976**, *47*, 2.
[35] K. C. Mills, B. J. Keene, *Slag Atlas*, 2nd edition, Verein deutscher Eisenhuettenleute, Verlag Stahleisen, Duesseldorf, Germany **1995**.
[36] C. W. Bale, E. Belisle, P. Chartrand, S. A. Degterov, G. Eriksson, K. Hack, I.-H. Jung, Y.-B. Kang, J. Melancon, A. D. Pelton, C. Robelin, S. Petersen, *Calphad* **2009**, *33*, 2.
[37] M. Song, Q. Shu, D. Sichen, *Steel Res. Int.* **2011**, *82*, 3.
[38] J. Goriupp, J. Schenk, G. Klösch, M. Hiebler, *Steel Res. Int.* **2014**, *85*, 4.
[39] A. Majdic, H. Wagner, *Arch. Eisenhüttenwesen* **1970**, *41*, 6.
[40] S. Maroufi, G. Ciezki, S. Jahanshahi, S. Sun, O. Ostrovski, *Metall. Mater. Trans. B* **2000**, *46*, 2.